10002–10017 *Nucleic Acids Research, 2017, Vol. 45, No. 17* *Published online 29 July 2017*
doi: 10.1093/nar/gkx666

TET2- and TDG-mediated changes are required for the acquisition of distinct histone modifications in divergent terminal differentiation of myeloid cells

Antonio Garcia-Gomez[1], Tianlu Li[1,†], Martin Kerick[2,†], Francesc Català-Moll[1], Natalia R. Comet[1], Javier Rodríguez-Ubreva[1], Lorenzo de la Rica[3], Miguel R. Branco[3], Javier Martín[2] and Esteban Ballestar[1,*]

[1]Chromatin and Disease Group, Cancer Epigenetics and Biology Programme (PEBC), Bellvitge Biomedical Research Institute (IDIBELL), 08908 L'Hospitalet de Llobregat, Barcelona, Spain, [2]Instituto de Parasitología y Biomedicina López-Neyra, Consejo Superior de Investigaciones Científicas (IPBLN-CSIC), Parque Tecnológico de La Salud (PTS), Granada, Spain and [3]Barts and The London School of Medicine and Dentistry, Centre for Neuroscience & Trauma, Blizard Institute, 4 Newark Street, London E1 2AT, UK

Received April 05, 2017; Revised July 03, 2017; Editorial Decision July 18, 2017; Accepted July 19, 2017

ABSTRACT

The plasticity of myeloid cells is illustrated by a diversity of functions including their role as effectors of innate immunity as macrophages (MACs) and bone remodelling as osteoclasts (OCs). TET2, a methylcytosine dioxygenase highly expressed in these cells and frequently mutated in myeloid leukemias, may be a key contributor to this plasticity. Through transcriptomic and epigenomic analyses, we investigated 5-methylcytosine (5mC), 5-hydroxymethylcytosine (5hmC) and gene expression changes in two divergent terminal myeloid differentiation processes, namely MAC and OC differentiation. MACs and OCs undergo highly similar 5hmC and 5mC changes, despite their wide differences in gene expression. Many TET2- and thymine-DNA glycosylase (TDG)-dependent 5mC and 5hmC changes directly activate the common terminal myeloid differentiation programme. However, the acquisition of differential features between MACs and OCs also depends on TET2/TDG. In fact, 5mC oxidation precedes differential histone modification changes between MACs and OCs. TET2 and TDG downregulation impairs the acquisition of such differential histone modification and expression patterns at MAC-/OC-specific genes. We prove that the histone H3K4 methyltransferase SETD1A is differentially recruited between MACs and OCs in a TET2-dependent manner. We demonstrate a novel role of these enzymes in the establishment of specific elements of identity and function in terminal myeloid differentiation.

INTRODUCTION

Myeloid cells undergo terminal differentiation processes in response to a variety of external stimuli that are exposed to in the bone marrow, blood and tissues. Myeloid terminal differentiation generates a great diversity of cell types including various macrophage types, inflammatory dendritic cells, osteoclasts and microglia among others. In these processes, the acquisition of a specific phenotype requires the exquisite regulation of gene expression, which depends on the interplay of receptors to extracellular signals, downstream signalling pathways and many different transcription and epigenetic factors. Myeloid cells express high levels of several epigenetic enzymes, like TET2 and DNMT3A, related to the modification of cytosines. This fact, together with the high frequency of mutations of these two enzymes in myeloid leukemias (1–3), indicates a key role of these processes in the specification of myeloid identity. Cytosine methylation is a major epigenetic mark associated with gene repression or activation and stability, depending on the genomic context (4). Cytosines can be not only methylated in the form of 5-methylcytosine (5mC), but also subsequently oxidized by Ten-Eleven-Translocation (TET) methylcytosine dioxygenases, thereby generating 5-hydroxymethylcytosine (5hmC), 5-formylcytosine (5fC) and 5-carboxylcytosine (5caC). The latter two are excised by thymine DNA glycosylase (TDG), triggering base excision repair that leads to the restitution of unmethylated cytosine (5). Alternative active DNA demethylation pathways have been reported involving the cytidine deaminase

*To whom correspondence should be addressed. Tel: +34 932607133; Fax: +34 932607219; Email: eballestar@idibell.cat
†These authors contributed equally to this work as second authors.

AID (6–8) or other DNA glycosylases (9,10). Methylated cytosines are specifically recognized by nuclear factors such as methyl-CpG binding domain proteins or Kaiso (11,12). These nuclear factors recruit histone modification enzymes to 5mC and locally modify the chromatin modification status (13,14). There is still some controversy about whether oxidized cytosines (5hmC, 5fC and 5caC) also have direct functional effects or merely act as intermediates. The latter two cytosine-oxidized forms, 5fC and 5caC, are present at low proportions, probably due to their instability or the fast turnover of the subsequent enzymatic steps (15). However, 5hmC is relatively stable (16) and is differentially recognized by certain nuclear factors (17–19). This suggests that it might be an epigenetic mark on its own merit. Recent data indicate that at least 5fC could also be a stable modification in mammals (20) with tissue-specific roles by recruiting specific transcriptional and chromatin regulators (19,21) or targeting active enhancers (20,22).

It is accepted that gene activation or transcriptional priming results from the tight crosstalk between cytosine methylation and histone modifications (23). It is likely not only that cytosine methylation interplays with complexes targeting histone modification but also that 5hmC and other oxidized cytosine forms have such effects. In connection with this, TET1–3 and TDG may not only have a role in active demethylation but also in modulating interactions between local chromatin and histone modification complexes based on the oxidation status of cytosines (24–26).

As aforementioned, myeloid cells undergo terminal differentiation processes that lead to the generation of various specialized cell types. These processes can be recapitulated *in vitro* from primary human MOs using related cocktails of growth factors such as GM-CSF or M-CSF, which lead to macrophage (MAC) differentiation. Additional cytokines like IL-4 and RANKL redirect MAC differentiation towards dendritic cell or osteoclast (OC) formation respectively. TET2-mediated oxidation of 5mC followed by TDG- and base excision repair-mediated recovery of unmethylated cytosines is essential in these monocyte (MO)-related differentiation processes (27,28). TET2 is targeted to specific genomic sites through specific transcription factors like PU.1 (29) or through IL-4-JAK3-STAT6 signalling (28). However, we know little about the functional contribution of TET2 and TDG in these myeloid differentiation processes and its contribution to the final phenotype beyond the effects on sets of genes.

To address these aspects, we first determined 5mC, 5hmC and expression changes over time in two related myeloid differentiation processes, namely MAC and OC differentiation. Differentiation to functional MACs and OCs is achieved *in vitro* using M-CSF in both cases, and RANKL is necessary for efficient differentiation of OCs. Despite their wide differences in gene expression, we observed that MAC and OC differentiation displayed very similar 5mC and 5hmC changes over time, indicating that RANKL makes a negligible contribution to the acquisition of DNA methylation profiles and that they mostly depend on M-CSF. By downregulating TET2 and TDG, we demonstrated that they are necessary for the acquisition of the final functional features of both MACs and OCs. In fact, we observed that a TET2- and TDG-mediated demethylation step is required before the differential acquisition of histone modifications like trimethylation of lysine 4 of histone H3 (H3K4me3) and acetylation of histone H3 (H3Ac) in genes that are differentially expressed between MACs and OCs. We also prove that TET2 is required to allow differential recruitment of the H3K4 methyltransferase SETD1A to OC-specific genes. This supports the notion that TET2 and TDG not only play a role in demethylating genes but also in ensuring the establishment of subsequent modification by histone modifications at specific genomic sites.

MATERIALS AND METHODS

Differentiation of MACs and OCs from peripheral blood mononuclear cells

Human blood samples used in this study came from anonymous donors via the Catalan Blood and Tissue Bank (CBTB) as buffy coats. All donors received oral and written information and signed a consent form prior to any donation at the CBTB. The CBTB follows the principles set out in the World Medical Association (WMA) Declaration of Helsinki. The blood was carefully layered on a Ficoll–Paque gradient (Amersham, Buckinghamshire, UK) and centrifuged at 800 g for 30 min without braking. After centrifugation, peripheral blood mononuclear cells (PBMCs) at the interface between the plasma and the Ficoll–Paque gradient were collected and washed twice with ice-cold phosphate-buffered saline, followed by centrifugation at 300 g for 5 min. Pure CD14+ cells were isolated from PBMCs using positive selection with MACS magnetic CD14 antibody (Miltenyi Biotec, Bergisch Gladbach, Germany). Cells were attached to the plate for 30 min in free-serum media and then cultured in α-minimal essential medium (α-MEM, Glutamax no nucleosides) (Invitrogen, Carlsbad, CA, USA) containing 10% fetal bovine serum, 100 units/ml penicillin, 100 μg/ml streptomycin and antimycotic and supplemented with 25 ng/ml human M-CSF (PeproTech EC, London, UK) for MAC differentiation. In the case of OC differentiation, we added soluble RANKL (50 ng/ml) (PeproTech EC, London, UK) in addition to M-CSF. Cells were seeded at a density of 1×10^6cells/well in 12-well plates and 1×10^5 cells/well in 96-well plates and cultured for 5 or 20 days (unless otherwise noted); medium and cytokines were changed twice a week.

Bisulfite (BS) and oxidative-bisulfite (oxBS) treatment

DNA was isolated by proteinase K protocol. BS and oxBS conversion were performed as detailed in Booth *et al*. (30). DNA samples (∼1 μg) were first purified with AMPure® XP beads (1.6× volumes) (Beckman Coulter Inc., CA, USA), washed with 80% ethanol and eluted in MilliQ-water. At this point, each DNA sample was split into two aliquots and processed through either the BS or oxBS treatment. The oxBS samples were purified via buffer exchange with Micro Bio-Spin® P-6 SSC columns (Bio-Rad Laboratories, Inc., USA) and eluted in ∼22 μl MilliQ-water. After DNA denaturation with 1.25 μl NaOH (1M) for 30 min in a shaking incubator at 37°C, DNA was oxidized with 2 μl $KRuO_4$ (15 mM) (Alfa Aesar, Germany) for 60 min in

an ice-water bath (vortexing the reaction twice) and centrifuged at 16 000 g for 15 min. Finally, both DNA and oxidized DNA were BS converted using the EZ DNA Methylation™ kit (Zymo Research, CA, USA). BS- and oxBS-modified DNA samples were then hybridized on the Infinium 450K chip or subjected to PCR amplification followed by pyrosequencing.

A spike-in 100-oligomer amplified with dhmCTPs (Bioline) was added to the DNA sample prior to preoxidation and interrogated by pyrosequencing to get accurate quantification of conversion efficiency (mean > 90%). Spike-in and pyrosequencing primer sequences are listed in Supplementary Table S1.

DNA methylation profiling using universal bead arrays

Infinium HumanMethylation450 BeadChips (Illumina, Inc., San Diego, CA, USA) were used to analyse 5mC and 5hmC levels. This array interrogates >485 000 methylation sites per sample at single-nucleotide resolution. This encompasses 99% of RefSeq genes, with an average of 17 CpG sites per gene region distributed across the promoter, 5′UTR, the first exon, the gene body and 3′UTR. It covers 96% of CpG islands, with additional coverage in CpG island shores and the regions flanking them. DNA samples were bisulfite-converted using EZ DNA methylation kits (Zymo Research, Orange, CA, USA). After bisulfite treatment, the remaining assay steps were performed following the specifications by the manufacturer. Arrays were hybridised using a temperature gradient program and imaged using a BeadArray Reader (Illumina, Inc.). Image processing and intensity data extraction software and procedures used were as previously described. Each methylation data point was obtained from a combination of the Cy3 and Cy5 fluorescent intensities from the M (methylated) and U (unmethylated) alleles. Background intensity correction was not used but fluorescent intensities close to zero were thresholded. For representation and further analysis we used beta and *M* values. Beta is the ratio of the methylated probe intensity to the overall intensity (the sum of the methylated and unmethylated probe intensities). Beta values range from 0 to 1, in which 0 is no methylation and 1 is complete methylation. Beta values show severe heteroscedasticity for highly methylated or unmethylated CpG sites and are therefore logistically transformed to *M* values, which were used to obtain FDR. Beta values were used to derive heatmaps and to compare DNA methylation percentages from bisulfite pyrosequencing experiments. For statistical purposes, the use of *M* values is more appropriate.

Quality control and data normalization

Methylation array data were processed in R using methods from the Bioconductor libraries minfi, lumi and limma. Data quality was assessed using the standard pipeline from the minfi package and no severe outliers were detected, although the BS and oxBS treated samples were observed to be distinct and were normalized separately. The normalization strategy was chosen comparing all available methods from the minfi package for lowest intra-group and highest inter-group variation. The data were quantile-normalized using a stratification approach including probetype (I, II), methylation ((un)-methylated), chromosome type (auto/gono-somes), sex (male/female) and CpG-region (CpG island, shore, shelf, open sea regions). After normalization, 5mC levels were derived from the oxBS data as beta values, while 5hmC levels were calculated by subtracting the oxBS *M* values from the BS *M* values using the same biological replicate. After subtraction, 5hmC *M* values were again quantile normalized and transformed to beta values. Negative 5hmC beta values were set to zero. The appropriate model was determined comparing different linear models for the 10K probes with highest variance across all individual data points ($n = 15$) using the selectModel function (limma package). Thirty two (42%) of CpG probes were best represented by the most complex model: methylation ~ individual + differentiation stage + error for the methylation and hydroxymethylation data, respectively. The data were analyzed using an eBayes-moderated *t*-test, available in the limma package, using the most complex model for all probes. To reduce the number of statistical tests we excluded probes that were unmethylated or fully methylated in all groups (0.15 > average beta > 0.8).

In this study, we considered a probe to be differentially methylated if it showed ≥2-fold (hypermethylation) or ≤0.5-fold (hypomethylation) changes. Additionally, only statistically significant tests ($P < 0.05$ and FDR < 0.05) were considered. For candidate gene selection we added the requirement for the difference in beta values to be at least 20% for the methylation and at least 10% for the hydroxymethylation data.

In vitro OC formation, pit formation and phagocytosis assay

The presence of OCs was checked at specified time points by tartrate-resistant acid phosphatase (TRAP) staining using the Leukocyte Acid Phosphatase Assay Kit (Sigma-Aldrich, Gillingham, UK) according to the manufacturer's instructions. TRAP+ multinucleated cells (≥3 nuclei) were considered as OCs and represented as a percentage of total cells (three randomly selected fields/well).To measure OC activity, MOs were seeded on calcium-coated wells (Corning, NY, USA) in osteoclastogenic medium for 20 days, and resorption pit area was calculated using the Adobe Photoshop histogram function (Adobe Photoshop CS5).

To quantify the phagocytic activity, MACs and OCs were detached using Cell Dissociation Solution Non-enzymatic (Sigma-Aldrich) and 50×10^3 cells were incubated with pHrodo™ red *E. coli* BioParticles® (Life Technologies, Oregon, USA) for 30 min at 37°C. Cells incubated on ice with BioParticles® were used as negative controls. Engulfed BioParticles® became fluorescent due to the acidic environment of the phagosome after phagocytosis and were detected at 585 nm by flow cytometry.

Flow cytometry analysis

Cells were detached using Cell Dissociation Solution Non-enzymatic (Sigma-Aldrich) and stained with fluorochrome-conjugated antibodies against CD163-FITC, CD11b-APC (both from BioLegend), CD206-FITC (BD BioSciences),

MSR1-Alexa Fluor® 700 (R&D Systems, MN, USA) and CD33-PE (eBioscience) at 5 and 20 days after M-CSF or M-CSF/RANKL stimulation. Cells (50×10^3) were acquired using a Gallios Flow Cytometer (Beckman Coulter, Pasadena, CA, USA) and analyzed by FlowJo software (Tree Star, Inc., Ashland, OR, USA).

Quantitative real-time PCR

Total RNA was isolated using TriZOL reagent (Qiagen). Reverse transcription was performed using the Transcriptor First Strand cDNA Synthesis Kit (Roche, Basel, Switzerland) according to manufacturer's instructions. qRT-PCR was done on a LightCycler® 480 II System using LightCycler® 480 SYBR Green Mix (Roche). Reactions were performed in triplicate for both the target and the housekeeping gene ribosomal protein L38 (*RPL38*) used for normalization. Relative quantification of the target gene expression was calculated by the comparative threshold cycle (Ct) method. Primer sequences are listed in Supplementary Table S1.

BS and oxBS pyrosequencing

DNA from BS and oxBS conversion (~20–30 ng) was used as a template in each subsequent PCR. Primers for PCR amplification and sequencing were designed with the PyroMark® Assay Design 2.0 software (Qiagen GmbH, Hilden, Germany). PCRs were performed with the HotStart Taq DNA polymerase PCR kit (Qiagen), and the success of amplification was assessed by agarose gel electrophoresis. PCR products were pyrosequenced with the Pyromark Q24 system (Qiagen). 5hmC levels were calculated by substraction of oxBS from BS methylation calls. All primer sequences are listed in Supplementary Table S1.

Gene expression arrays

Expression studies were performed using the Agilent platform following manufacturer's instructions. Briefly, 100 ng RNA extracted with TriZOL from MOs, MACs and OCs hybridized to a SurePrint G3 Human Gene Expression Array (Agilent Technologies, CA, USA). Probe intensity normalization and downstream analysis were obtained using statistical analysis language R in combination with Bioconductor repository functions (http://bioconductor.org). Data normalization was followed by probe identity filtering, under strong statistical confidence thresholds ($P < 0.01$; FDR < 0.05; FC < 0.5 and FC > 2 for downregulated and upregulated respectively). Finally, comparison of expression and DNA methylation and hydroxymethylation data were performed by applying custom R scripting. To test for the association of gene expression and 5mC/5hmC we calculated the Pearson correlation coefficient using outlier corrected data. In detail, we fit a linear model and removed data points with Cooks distance measures greater than twice the median Cooks distance.

Gene ontology analysis

Gene ontology (GO) was analyzed with the FatiGO tool (31), which uses Fisher's exact test to detect significant over-representation of GO terms in one of the sets (list of selected genes) with respect to the other (the rest of the genome). Multiple test correction to account for the multiple hypotheses tested (one for each GO term) was applied to reduce false-positive results. GO terms with adjusted values of $P < 0.05$ were considered significant.

Enhancer identification and HOMER analysis

Enhancers were identified using the FANTOM5 Transcribed Enhancer Atlas that is available online (http://fantom.gsc.riken.jp/5/top). This tool allows the identification of distinct bidirectional Cap Analysis of Gene Expression (CAGE) patterns to predict the existence of enhancers in a variety of human cells including monocytes. The search for transcription factor sequence recognition motifs was performed using HOMER software v4.5. To determine the relative enrichment of known motifs in CpGs mapping in enchancer regions for each cluster, sequence contained in 500-bp windows was searched against a selected background of windows that were adjusted to have equal GC content and the same number of CpGs.

Immunoblotting

Electrophoresis and immunoblotting were performed according to standard procedures. The blots were developed using the ECL detection kit (Amersham Pharmacia Biotech Inc., NJ, USA). Primary antibodies were directed against: TET2 (Diagenode, Ref: C15200179), TDG (kindly provided by Dr P. Schär, from the University of Basel), histone H3 (Abcam, Ref: ab1791) and actin (Abcam, Ref: ab6276).

Chromatin immunoprecipitation (ChIP) assays

For ChIP assays, MOs, MACs and OCs were crosslinked at specified differentiation day with 1% formaldehyde and subjected to immunoprecipitation after sonication. ChIP experiments were performed using the LowCell# ChIP kit™ protein A (Diagenode, Liège, Belgium) and antibodies against acetylated Lys at the N-t of histone H3 (H3Ac) (Millipore, Ref: 06-599), trimethylated Lys 4 of histone H3 (H3K4me3) (Millipore, Ref: CS200580) and histone H3 Lys 4 methyltransferase SETD1A (Abcam, Ref: ab70378). Analysis was performed by real-time quantitative PCR. Data are represented as the ratio of the 'bound' fraction of the histone modification antibody with respect to the input. ChIP primers were designed for the areas flanking differentially methylated CpGs and their sequences are shown in Supplementary Table S1.

Transfection of primary human MOs

We used ON-TARGETplus siRNAs (GE Healthcare Dharmacon) against TET2, TDG and AICDA to perform knockdown experiments in peripheral blood MOs. We also used ON-TARGETplus Non-targeting Control Pool as a negative control. We transfected MOs with siRNAs using Lipofectamine 3000 Reagent (Thermo Fisher Scientific Co., Carlsbad, CA, USA). We repeated transfections every 3 days after starting the culture. We examined the levels of the target factors by qRT-PCR and western blot assays at specified times.

Statistical analysis

Each assay was performed at least three times using MOs from different individuals. Quantitative data are expressed as mean ± SEM. Data were analyzed using GraphPad prism software Version 6 (GraphPad). Statistical comparisons were performed using the nonparametric Mann–Whitney U test (2 groups) and Kruskal-Wallis with Mann–Whitney *U* post-hoc test, and values of $*P < 0.05$ were considered significant (GraphPad Software Inc., CA, USA).

RESULTS

MACs and OCs display almost identical 5mC and 5hmC profiles that depend on M-CSF stimulation

To investigate the role of TET2-mediated changes in terminal myeloid differentiation, we first performed in parallel mRNA, 5mC and 5hmC profiling of two related myeloid differentiation processes, specifically MAC and OC differentiation, which produce two morphologically and functionally distinct cell types. MO-to-MAC and MO-to-OC differentiation depend on M-CSF stimulation, and the latter requires the additional factor RANKL (Figure 1A). Specifically, we analyzed MOs stimulated for 5 and 20 days with M-CSF and M-CSF/RANKL.

TRAP staining, dentin resorption and phagocytic activity assays confirmed the acquisition of function. At 5 days, both M-CSF and M-CSF+RANKL cultures were stained positive for TRAP and had a similar appearance containing a high number of spindle-like cells without displaying cell fusion (Supplementary Figure S1A). However, at 20 days only MOs incubated with both M-CSF and RANKL differentiated into giant polykaryons (>80% with 3–20 nuclei) with a large cytoplasmic spreading and resorption activity, as expected for OCs (Figure 1B). In contrast, only a small number (<10%) of M-CSF treated MOs displayed cell fusion (3–5 nuclei) as previously reported (32). The phagocytic activity of MOs treated with M-CSF for 20 days was significantly higher than in those treated with both M-CSF and RANKL (Figure 1C). FACS analysis confirmed the existence of differential surface marker staining in MOs, MACs and OCs. The scavenger receptor CD163 showed significantly higher expression levels in MACs compared to OCs after 20 days of cytokine stimulation, whereas M2 macrophage markers (CD206 and MSR1) and myeloid markers (CD33 and CD11b) were increased in both cell types during the differentiation process (Figure 1D).

Expression profiling of MACs and OCs at 5 and 20 days allowed the identification of transcripts that are differentially expressed (Supplementary Figure S1B). Specifically, we observed upregulation of 4339 and 4513 genes and downregulation of 3110 and 3098 genes 5 days after stimulation with M-CSF- and M-CSF/RANKL, respectively (>2-fold change or <0.5-fold change; $P < 0.01$; FDR < 0.05) (Supplementary Table S2). The comparison between MOs stimulated for 5 and 20 days showed that 1342 and 1241 were upregulated, and 1064 and 1370 were downregulated with M-CSF and M-CSF/RANKL stimulation, respectively (Supplementary Table S2), indicating that major expression changes occurred during the first 5 days of differentiation. In this analysis, we also observed differences in gene expression between MACs and OCs at 5 and 20 days (Figure 1E and Supplementary Figure S1C). Differences were noted in genes such as *FOLR2*, *IL10, C1QC* and *VSIG4* (involved in the modulation of the inflammatory response), which show higher expression in MACs compared to OCs (33). Upregulated genes in OCs included *CTSK*, *ADAMTS14* and *MMP1* (encoding for proteases involved in bone matrix resorption), whereas the transcription factor *IRF8* was specifically downregulated in OCs, in accordance with its repressive role in this context (34) (Figure 1F). In brief, all these analyses confirmed the wide range of differences between these two differentiated cell types.

For 5mC and 5hmC profiling, we hybridized BS- and oxBS-treated DNA samples (MOs, 5 days MACs and pre-OCs, 20 days MACs and OCs) on bead arrays. Statistical analysis of the combined data from the five sets of samples ($\Delta\beta > 0.2$; $P < 0.05$; FDR < 0.05 for 5mC; $\Delta\beta > 0.1$; $P <$ 0.05 for 5hmC) (Supplementary Table S3 and Supplementary Table S4) yielded several initial conclusions, which are summarized as follows: (i) the patterns of both 5mC and 5hmC of M-CSF- and M-CSF/RANKL-stimulated MOs are highly similar at both 5 and 20 days, indicating that RANKL makes a small contribution to the acquisition of changes in the 5mC and 5hmC patterns (Figure 2A and E); (ii) both MAC and OC differentiation predominantly undergo loss of 5mC (Figure 2A), whereas gains of 5mC only occur at late stages in both processes (Figure 2A); (iii) 5hmC dynamics are more complex than those of 5mC, and 5hmC changes include groups of CpG sites that lose 5hmC, in contrast to other groups of CpG-containing sequences that undergo transient or permanent gains of 5hmC (Figure 2E).

Firstly, RANKL did not have a drastic effect on the acquisition of differential methylation patterns (Figure 2A) in contrast to the effects observed in similar processes by other cytokines like IL-4 (28). By decreasing the threshold ($\Delta\beta >$ 0.1) we were able to identify around 55 CpG hypomethylated in OCs with respect to MACs and only 6 CpG sites were hypermethylated in OC with respect to MACs at 20 days following M-CSF (and RANKL) stimulation (Supplementary Figure S2A and Supplementary Table S5). The majority of these changes are located in *open sea* regions encompassing gene body and intergenic regions (Supplementary Figure S2B, left). GO analysis identified significant enrichment in functions related to OC biology, (Supplementary Figure S2B, right) and HOMER analysis revealed putative TF binding motifs such as Jun/Fos, BATF or ZNF528 (Supplementary Figure S2C). These small 5mC changes across cell differentiation affected genes involved in proteolytic activity (*CTSK, ADAMTS8, HYAL2*) and related with NF-κB regulation (*URGCP* and *WDFY1* as activators and *ZNF366, SLC39A1* and *CUX1* as inhibitors) (35–37). Bisulfite pyrosequencing of representative CpGs (*CTSK* and *ZNF366*) confirmed their demethylation in OCs, but also some partial demethylation in MACs (Supplementary Figure S2D), suggesting that the observed differences may be indirect rather than the result of specific targeting by elements downstream of RANKL. Most DNA methylation changes in both MAC and OC differentiation therefore appeared to depend on M-CSF, which, upon interaction with its receptor M-CSFR, mediates downstream effector functions. In fact, treatment of MACs and OCs with

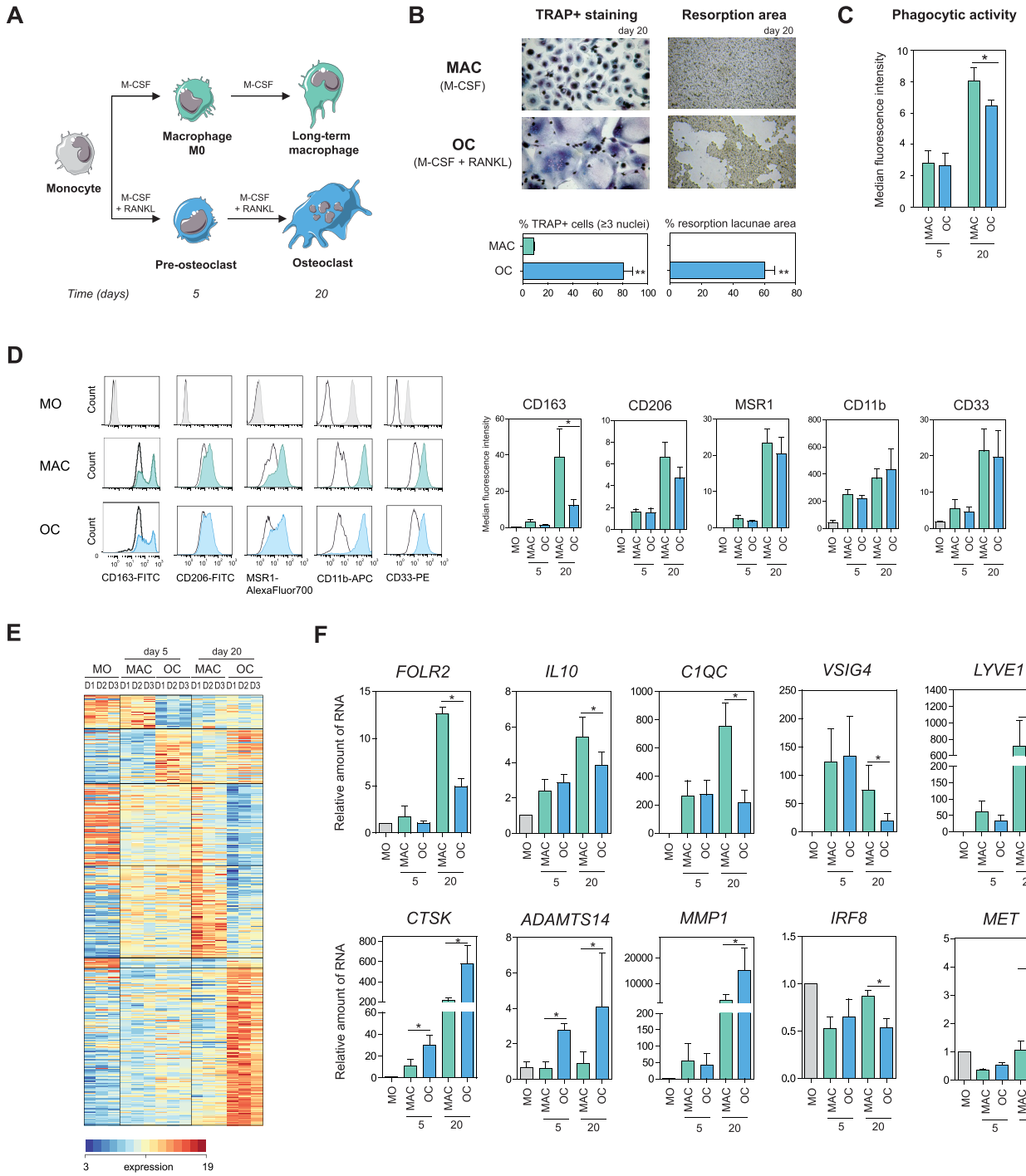

Figure 1. M-CSF and RANKL drive differential gene expression and function in MACs and OCs. (**A**) Schematic diagram depicting the two cell differentiation processes. Peripheral blood MOs are either stimulated with M-CSF or M-CSF/RANKL to generate MACs and OCs, respectively. At 5 days, M-CSF cells are fully differentiated into MACs, whereas M-CSF/RANKL cells are pre-OCs (not displaying cell fusion); at 20 days, OCs have achieved full differentiation. (**B**) TRAP staining and pit resorption analysis of M-CSF- and M-CSF/RANKL-treated cells at 20 days. At the bottom, a bar graph representing the percentage of OCs (TRAP+ cells with three or more nuclei) (left) and a bar graph representing the percentage of the resorption lacunae area (right) are presented. (**C**) Phagocytosis assay showing the fluorescence emission of engulfed bacteria by MACs and OCs at 5 and 20 days. (**D**) Analysis of MAC and OC surface markers (CD163, CD206, MSR1, CD11b and CD33) by flow cytometry. Histograms show the percentage of positive cells for each marker (left) and graphs show the median fluorescence intensity (MFI) for selected surface markers (right). (**E**) Heatmap including all the genes displaying significant expression changes between MAC and OC at 5 and 20 days (>2-fold or <0.5-fold change; $P < 0.01$ and FDR < 0.05). A scale is shown at the bottom, wherein expression values range from -3 (lower expression levels, blue) to +3 (higher expression levels, red). (**F**) Expression of MAC (*FOLR2, IL10, C1QC, VSIG4, LYVE1*) and OC (*CTSK, ADAMTS14, MMP1, IRF8, MET*) markers, checked by quantitative RT-PCR at 5 and 20 days in comparison with MOs. Quantitative RT-PCR data relative to RPL38. Graphs represent mean values from MACs and OCs derived from MOs of three healthy donors ± SEM. *$P < 0.05$ indicates significant differences between M-CSF and M-CSF+RANKL-treated cultures.

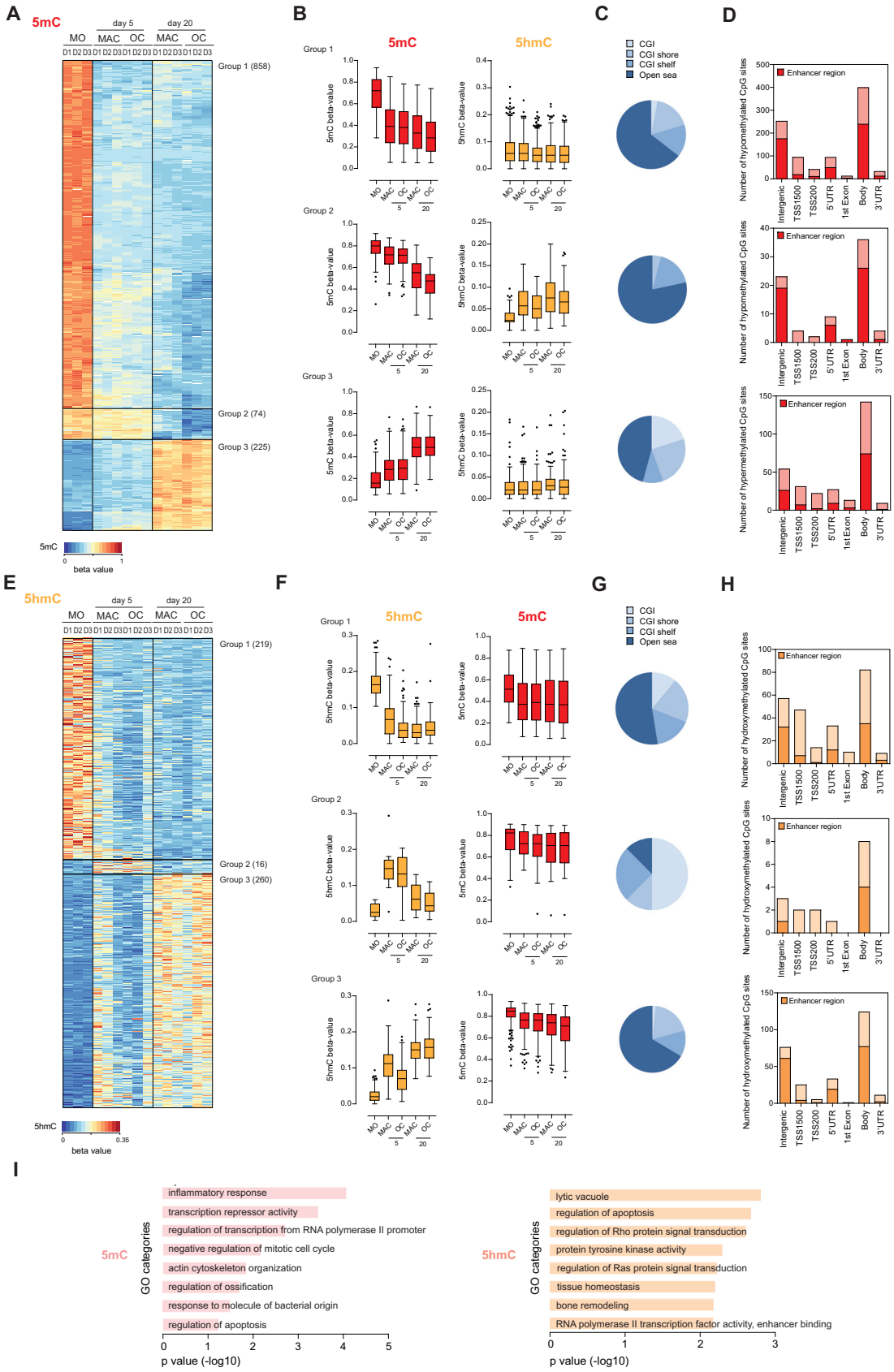

Figure 2. High-throughput 5mC and 5hmC profiling in MOs following M-CSF and M-CSF/RANKL exposure leading to MACs and OCs respectively. (**A**) Heatmap including the 5mC data for three paired samples of MOs, MACs and OCs (D1, D2, D3) harvested on days 5 and 20. The heatmap includes all CpG-

GW2580, an M-CSFR inhibitor, led to a significant impairment of demethylation changes in selected genes including *FOXP1* and *IL10* (Supplementary Figure S2E).

Different 5hmC dynamics during MAC and OC differentiation are associated with loss of 5mC

The analysis of the 5mC patterns in MOs following 5 and 20 days of M-CSF or M-CSF/RANKL exposure revealed the existence of three clusters of CpG sites (Figure 2A): group 1–5mC, corresponding to 858 CpG sites that undergo a rapid loss of 5mC; group 2–5mC, comprises of 74 CpG sites that undergo a slow loss of 5mC, which was only significant at day 20; group 3–5mC, a cluster of 225 CpG sites that undergo gains of 5mC (Supplementary Table S3). This latter finding showed that gains of DNA methylation are not exclusive to OCs (28,29) but also occur in MACs when M-CSF stimulation is maintained for several weeks. We then investigated the corresponding 5hmC levels for the same CpG sites in the groups that displayed differential 5mC profiles during the two differentiation processes and observed that the CpGs that underwent a slow loss of 5mC achieved a significant increase in 5hmC in both MACs and OCs at 5 and 20 days (Figure 2B). As expected, hypermethylated CpGs exhibited the lowest levels of 5hmC (Figure 2B). In general, changes in 5mC are not necessarily associated with changes in 5hmC for the indicated times of the differentiation process.

When focusing the analysis on 5hmC changes (Figure 2E), we also observed the appearance of three groups of CpG sites: group 1–5hmC, corresponding to a group of CpG sites that display higher levels of 5hmC in MOs and undergo loss of 5hmC over time at 5 and 20 days; group 2–5hmC are CpG sites that display a transient increase in 5hmC at 5 days followed by a decrease at 20 days; group 3–5hmC is a cluster of CpG sites that undergo increases in 5hmC and remain relatively high over time (Figure 2E and Supplementary Table S4). Groups 1 and 3 represent CpG sites that have stable high levels of 5hmC in MOs or in the final MAC/OC differentiated state, suggesting that 5hmC is a stable epigenetic mark. We observed that the three groups of CpG sites displaying changes in 5hmC are generally associated with CpG sites that undergo a loss of 5mC (Figure 2F).

With respect to the relationship of these changes to CpG islands, most 5mC changes occurred at *open sea* areas for CpG displaying slow or fast hypomethylation, whereas hypermethylated CpGs were additionally enriched in CpG islands and shores. Consistent with previous studies (38–40), we detected an accumulation of 5hmC at locations outside of CpG island regions, except for group 2 of 5hmC (transient increase in 5hmC), which were enriched in CpG islands (or in the near vicinity) (Figures 2C and G). The majority of CpG sites undergoing 5mC and 5hmC changes occurred at promoters gene bodies in both cases, in concordance with other studies (41,42) (Figure 2D and H). According to previous sequencing data for ESCs, 5mC and 5hmC is also abundant at enhancer regions (39). Gene ontology analysis of CpG sites displaying 5mC and 5hmC changes (Figure 2I) revealed the enrichment of functional categories associated with the inflammatory response, the response to molecules of bacterial origin and bone remodeling, among others, which are related to MAC and OC biology.

Gains or losses of 5hmC positively correlates with gene expression during terminal myeloid differentiation

For genes undergoing common changes in 5mC during MAC and OC differentiation, which make up the vast majority, we compared the 5mC and 5hmC datasets with the expression data, focusing on genes that underwent significant demethylation. For genes that experienced significant changes in 5mC, we explored their gene expression, analysing the aforementioned three groups of sequences (group 1, genes undergoing rapid loss of 5mC; group 2, genes undergoing slow loss of 5mC; group 3, genes displaying gains of methylation). Group 1–5mC genes had a positive correlation with gene expression in CpG shores and promoters, while group 2–5mC genes displayed a positive correlation with expression in *open sea* regions (Supplementary Figure S3). For group 3–5mC genes, gains of methylation at CpG sites in CpG shores, shelves, *open sea* regions and gene bodies displayed a negative correlation (Supplementary Figure S3A), in accordance with previous studies (43).

In a similar way, we investigated the relationship between 5hmC changes and gene expression, considering the 5hmC dynamics of the three groups. We observed that some significant correlations between 5hmC and mRNA levels. For instance, for genes in group 1–5hmC (high levels in MOs, low in MACs/OCs) we observed a positive correlation be-

←

containing probes displaying significant methylation changes (a total of 1157 with $\Delta\beta > 0.2$, $P < 0.05$ and FDR < 0.05) (data in Supplementary Table S3). A scale of beta values (i.e. the ratio of the methylated probe intensity to the overall intensity, where overall intensity is the sum of methylated and unmethylated probe intensities), ranging from 0 (unmethylated, blue) to 1 (completely methylated, red), is shown at the bottom. (**B**) Box-plots corresponding to the 5mC-normalized data (left) and 5hmC-normalized data (right) for each of the groups presented in the heatmap in the previous section. (**C**) Distribution of 5mC in relation to CpG islands (CGI), including shores, shelves and *open sea* regions for each of the groups of CpG sites in section A. (**D**) Distribution of 5mC organised by genomic location (intergenic, promoter (1500 and 200 upstream of the TSS, 5′UTR, first exon, gene body, and 3′UTR) for each of the groups of CpG sites in section A. The darker insets within each bar indicate the number of sites annotated as enhancers. (**E**) Heatmap including the 5hmC data for three paired samples of MOs, MACs and OCs (D1, D2, D3) harvested on days 5 and 20. The heatmap includes all CpG-containing probes displaying significant methylation changes (a total of 495 with $\Delta\beta > 0.1$ and $P < 0.05$) (data in Supplementary Table S4). A scale of beta values is shown at the bottom. (**F**) Box-plots corresponding to the 5hmC-normalized data (left) and 5mC-normalized data (right) for each of the groups presented in the heatmap in the previous section. (**G**) Distribution of 5hmC in relation to CpG islands (CGI), including shores, shelves and *open sea* regions for each of the groups of CpG sites in section E. (**H**) Distribution of 5hmC organised by genomic location (intergenic, promoter 1500 and 200 upstream of the TSS, 5′UTR, first exon, gene body, and 3′UTR) for each of the groups of CpG sites in section E. The darker insets within each bar indicate the number of sites annotated as enhancers. (**I**) Gene ontology (GO) enrichment analysis of CpG sites undergoing 5mC (left) or 5hmC (right) changes in differentiation to MAC and OC.

tween 5hmC and mRNA levels (Figure 3A, left). Looking at CpG sites from group 3–5hmC (low levels in MOs, high in MACs/OCs), we also observed positive correlations with gene expression for those located in promoters and gene bodies, as well as CpGs located in CGI shores and *open sea* regions (Figure 3A, right). In all these cases, therefore, high levels of 5hmC associate with high mRNA levels.

We further investigated the relationship between genes with high levels of 5hmC in MOs (group1–5hmC) or in MACs/OCs (group3–5hmC) and genes that are highly expressed in MOs and MACs/OCs. This analysis revealed the existence of two sets of genes corresponding to key functions for MOs or to the common functions in MACs/OCs (Supplementary Table S7). For genes in group1–5hmC, loss of 5hmC associated with decreased mRNA levels in genes like *ICAM3*, *CD300E* and *BCL6*, although other genes experienced increased expression such as *ANXA2* or *CD59* (Figure 3B). For genes in group3–5hmC, increase in expression was more robust and involved key genes associated with proper differentiation and function of OCs (*ACP5*, *PLD1* and *S100A3)* and MACs (*CSF1R*, *MITF* and *SLAMF8*). Changes in 5hmC may be necessary to maintain the high levels of core genes controlling MO and MAC/OC function. Analysis of 5mC and 5hmC changes of selected key genes from the different groups over time during OC differentiation confirmed that the three different 5hmC dynamics (loss, transient gains, permanent gains) were associated with loss of 5mC, although expression changes were specific to each gene, providing further evidence that additional mechanisms ensure the specificity for each particular gene (Figure 3B). Furthermore, upon the inspection of the 5mC methylation status of distinct enhancers that fall in 5mC groups 1–3, we observed that enhancer hypermethylation (group 3–5mC) correlates with a decrease in the expression of paired genes (Supplementary Figure 3B and C), following enhancer-promoter pairing analysis. HOMER motif analyses of differentially methylated enhancers revealed the enrichment of several important transcription factors, including those belonging to the bZIP family, which further supports the notion that gene expression changes may require additional mechanisms (Supplementary Figure 3D).

Downregulation of TET2 and TDG impairs transcriptional activation in genes undergoing 5hmC changes as well as affect the stability of the final phenotype

Next, we interrogated the role of TET2 and TDG in these differentiation processes. Additional enzymes in the TET-related pathway towards demethylation potentially involve other TET family members and TDG (and other DNA glycosylases, including MBD4). It has also been reported that activation-induced deaminase (AID) and other related enzymes could deaminate 5mC and/or 5hmC (Figure 4A) (44) followed by the participation of TDG, but this possibility is still controversial (45). We therefore inspected the mRNA expression levels of these enzymes in MOs and cells stimulated with M-CSF and M-CSF/RANKL at 5 and 20 days (Figure 4B). Our data confirmed that TET2 is the only gene of the TET family expressed in these cells. Also, the glycosylases TDG, MBD4, MPG, UNG or SMUG1 and the cytidine deaminases AID, APOBEC3A, APOBEC3B and APOBEC3F are expressed in these MOs, MACs and OCs. Some of these enzymes have been proposed as mediators of DNA demethylation in other contexts (7,8,46). We measured the levels of some of these proteins over time using qRT-PCR and western blot (Figure 4C). Based on these data and the existing literature we decided to focus on the DNA demethylation pathway based on TET2-subsequent oxidation followed by TDG-mediated removal and also to explore the role of AID in active demethylation.

First, we investigated the effects of downregulating TET2, TDG and AID on the acquisition of MAC and OC identity and function. Interestingly, all three affected the ability of M-CSF/RANKL-treated MOs to become functional OCs, as demonstrated using TRAP staining and dentin resorption assays (Figure 4D). We also showed that these enzymes partially impair phagocytic activity and the ability to acquire some of the MAC surface markers (Figure 4D).

Second, we tested the effects of the downregulation of the *TET2*, *TDG* and *AICDA* genes on the dynamics of 5mC and 5hmC changes and the expression of genes from the different groups, as well as the ability of MOs to correctly differentiate into OCs (similar analysis was performed for MAC differentiation, not shown). Downregulation of TET2 resulted in accumulation of both 5mC and 5hmC (Figure 4E), the latter perhaps as a result of defective further oxidation of 5hmC to 5fC and 5caC, and a decrease in the activation of genes (Figure 4F) from the three groups with different 5hmC dynamics. In the case of TDG siRNA-mediated downregulation, we observed a delay in the loss of methylation, possibly as a result of the defective processing of the oxidized cytosines into abasic sites that leads to accumulation of 5mC and 5hmC (Figure 4E and F). In this case, we also observed a delay in the expression of the analyzed genes. Interestingly, we observed a similar effect with the siRNA for AID, although only for some of the genes (Figure 4E, F and Supplementary Figure S4B), supporting a participation in this process.

In summary, these results suggest that TET2, TDG and, in some cases AID, act together in the regulation of common genes in MAC and OC differentiation as well in the acquisition of their final phenotypes.

Differential gene expression between MACs and OCs is related to differential histone modification patterns and require prior TET2 and TDG participation in both processes

To assess the functional consequences of TET2 and TDG in relation to differential gene expression profiling, we first explored the CpG methylation status of genes that are differentially expressed between both myeloid cell types.

First, with respect to the genes that are differentially expressed between OCs and MACs (Supplementary Table S2), we observed a significant correlation between 5mC changes and gene expression for the indicated comparisons, where DNA hypomethylation or hypermethylation associates with gene upregulation or downregulation respectively (Figure 5A). The largest cell type-specific expression changes occurred during the first step of differentiation (Figure 5A), and the majority of DNA methylation

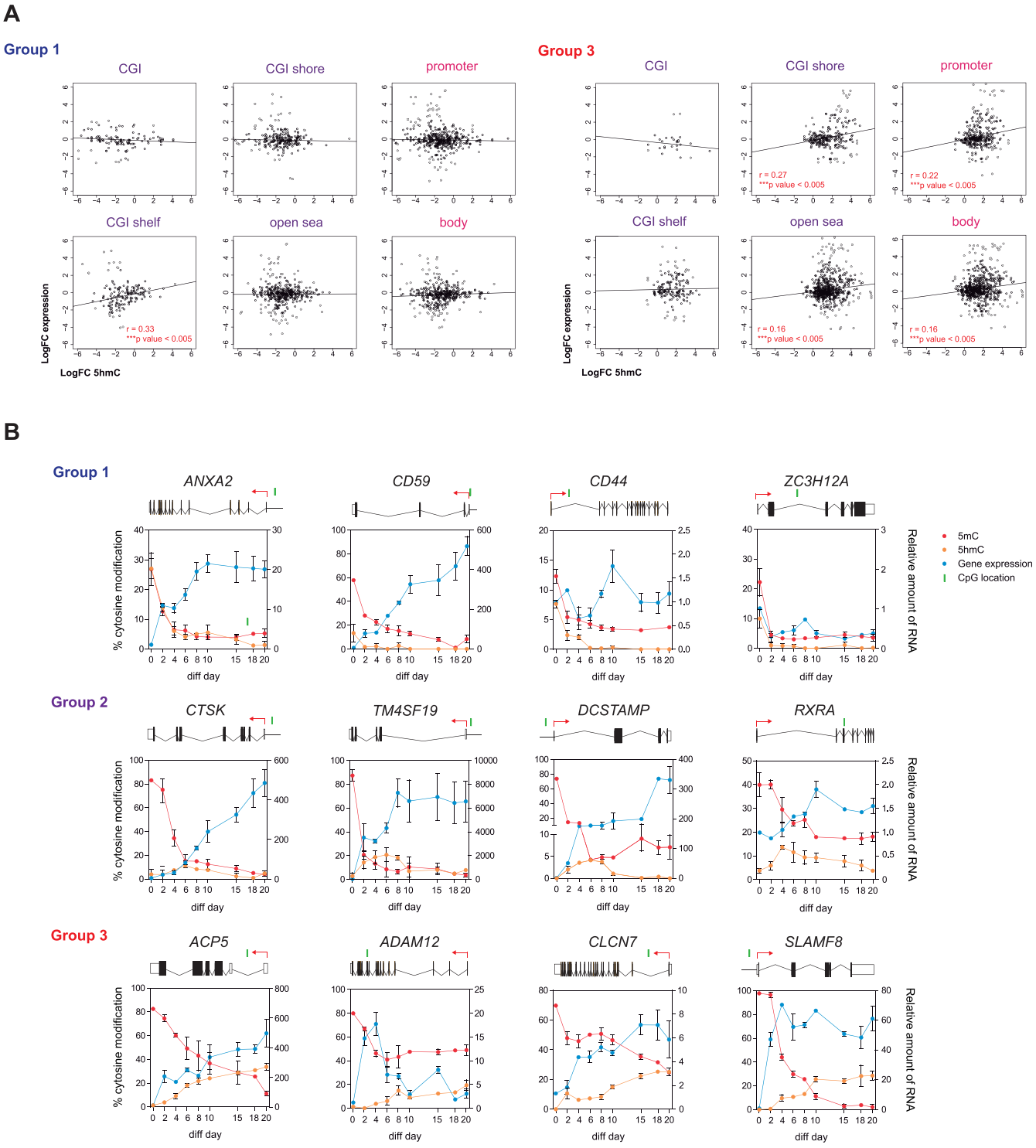

Figure 3. Correlation between DNA hydroxymethylation signatures and gene expression during MAC and OC differentiation. (**A**) Scatterplots showing the relationship between the $\log_2$FC in gene expression and the $\log_2$FC in 5hmC for all the genes which display significant 5hmC changes across the MAC and OC differentiation. Correlation are grouped between CpG sites undergoing rapid loss of 5hmC from MOs (group 1, left) and CpG sites displaying gains of 5hmC in MAC and OC differentiation at day 20 (group 3, right). Scatterplots are organized by genomic location [promoter (1500 and 200 upstream of the TSS + 5′UTR + first exon) and gene body] and relation to CpG island (shore, shelf and *open sea*). (**B**) 5mC, 5hmC and gene expression dynamics of selected CpG during monocyte-to-OC differentiation. 5mC and 5hmC are determined by the combination of bisulfite (5mC+5hmC) and oxidative bisulfite (5mC) pyrosequencing. Quantitative RT-PCR data is normalized against *RPL38*. 5mC, 5hmC and gene expression data are represented with red, orange and blue lines, respectively.

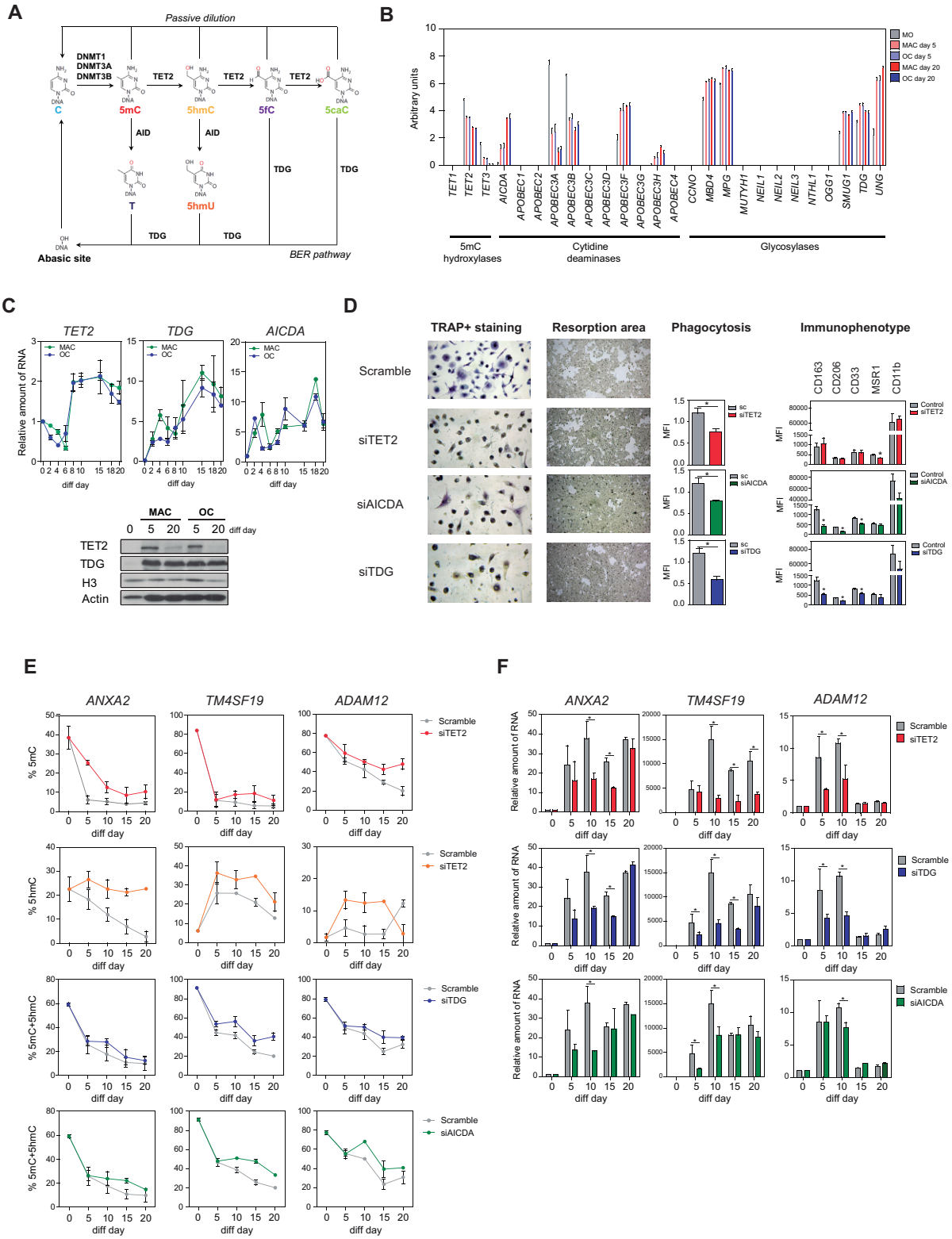

Figure 4. TET2 and TDG regulate active DNA demethylation and gene expression in MAC and OC differentiation. (**A**) A schematic representation depicting the participation of enzymes including DNA methyltransferases (DNMT1, DNMT3A and DNMT3B), methylcytosine dioxygenases (TET2), thymine DNA glycosylases (TDG) and the base excision repair machinery (BER pathway) in the oxidation and demethylation of cytosines. (**B**) Gene expression levels of several enzymes (or related family members) associated with active DNA demethylation are evaluated in MOs and differentiated MACs and OCs at 5 and 20 days of differentiation. These enzymes are grouped as 5mC hydroxylases, cytidine deaminases, or glycosylases based on their described activity during the demethylation process. (**C**) mRNA levels of *AICDA*, and mRNA and protein levels of TET2 and TDG are evaluated in MOs and differentiated MACs and OCs during 20 days. Quantitative RT-PCR data is normalized against *RPL38*. Histone H3 and actin levels are used as a

changes corresponded to hypomethylated CpGs (69,3%) located at promoter regions (42,2%) but also in gene bodies (50%) (Supplementary Table S6). This suggests that expression differences between these two cell types may depend on the 5mC status but not necessarily related to the establishment of differential DNA methylation changes. Alternative mechanisms may account for differential RANKL-mediated expression of these genes, such as regulation of post-translational modifications of the residues of histones and chromatin structure. To explore the potential role of histone modification patterns in differentially gene expression between both cell types, we selected several MAC- (*IL10*, *VSIG4, LYVE1*) and OC-upregulated (*CTSK*, *PLD1, S100A3*) genes (Figure 1 and Supplementary Table S2) and performed ChIP assays to test enrichment in acetylated Lys at the N-t of histone H3 (H3Ac) in these genes. This experiment showed that OC-specific genes like *CTSK*, *PLD1* or *S100A3* are more enriched in H3Ac in OCs than in MACs, whereas the opposite was observed for MAC-specific genes like *IL10*, *VSIG4* and *LYVE1* at 20 days (Figure 5B). However, we did not observe differences in H3Ac at day 5, corresponding with no changes in their gene expression (Figure 1 and Supplementary Table S2). Using ChIP-seq data from Blueprint database, we also compared the BS-seq data and the ChIP-seq profiling of the active chromatin marker H3K4me3 in MO, MACs and OCs, confirming the differential H3K4me3-enriched regions for our differentially expressed genes in both cell types (Figure 5C and Supplementary Figure S5).

This differential histone modification pattern is not necessarily related to DNA methylation differences between the two cell types, although a common prior M-CSF-related demethylation step may play a role in conferring the competence of these genes to acquire histone modification marks compatible with their activation changes. To address the question to whether active DNA demethylation machinery harbour regulatory functions in histone modification changes, we examined the effect of TET2 and TDG in histone modifications known to control gene activation such as H3Ac or H3K4me3. We observed that either H3Ac or H3K4me3 had differential increased levels in MACs or OCs with respect to MOs (Figure 5) Downregulation of TET2 and TDG with siRNAs not only showed a reduction in H3Ac and H3K4me3-enriched demethylated genes (Figure 5D) but also resulted in specific reduction in the acquisition of expression changes at those target genes (Figure 5E).

TET2-mediated changes are required for the specific recruitment of the H3K4 methyltransferase SETD1A

Finally, to investigate the specific role of TET2-mediated changes in the subsequent recruitment of histone modification enzymes, we decided to focus on those related to H3K4me3, one of the two modifications previously studied. We first checked the global mRNA levels of several H3K4 methyltransferases, namely MLL1–5, SETD1A and SETD1B, and demethylases, including KDM1A, KDM1B and KDM5A-D, during MAC and OC differentiation. Following differentiation, we observed a downregulation of methylases, whereas the majority of demethylases become upregulated. Next, we mediated the knockdown of TET2 by siRNA and we observed that the majority of the H3K4 modifying enzymes remain unaffected, while only KDM1A and KDM1B suffered a slight but significant downregulation in OCs compared to MACs (Figure 6A). We then focused on the recruitment of SETD1A, the catalytic subunit of the SET1/COMPASS complex which mediates bulk methylation of H3K4 and whose binding has been reported to be linked to TET2/3 activity (24) to selected genes such as *CTSK*, *PLD1* and *S100A3*. First, we observed that SETD1A is indeed bound to these genes in OC and to a lower extent in MACs. Second, we showed that TET2 knockdown impairs SETD1A binding in OCs, demonstrating the presence of TET2 is required for the recruitment of the H3K4 methyltransferase SETD1A to mediate the appropriate methylation of histones at OC-specific genes (Figure 6B).

DISCUSSION

Our results demonstrate that TET2 and TDG are essential at least at two different levels for the acquisition of the terminal myeloid phenotype, exemplified by MAC and OC differentiation. TET2 and TDG not only participate in mediating 5hmC and 5mC changes that are common to both processes but also allow the subsequent occurrence of acquisition of differential histone modifications at MAC- and OC-specific genes. Differential enrichment in activating histone modifications H3Ac and H3K4me3 account for differential changes in expression of some genes between MACs and OCs. For some of these genes, we prove that a common prior demethylation event has to take place before differential expression and histone modification profiles are achieved. We also show that binding of H3K4 methyltransferase SETD1A to these genes depends on TET2. Also, 5hmC profiling over time reinforces the notion that this modification is stable, and our data indicates that it has a direct role in stabilising final myeloid identity and function.

The broad similarities between the methylomes and hydroxymethylomes of MACs and OCs at 5 and 20 days suggest that these profiles are not directly associated with the distinctive features of these two cell types. These data, together with the results obtained following the impact on DNA demethylation of these cells treated with an inhibitor of M-CSFR, indicate that changes in 5mC and 5hmC do not depend on RANKL and that they can be attributed

←

loading control in the western blot. (**D**) The effects of siRNA-mediated downregulation of TET2, TDG and AID are evaluated in OCs and MACs. TRAP staining and dentin resorption assays (left panels) are performed in OCs after 20 days of differentiation. Phagocytosis assays and FACS analyses of surface markers, including CD163, CD206, MSR1, CD11b and CD33 (right panels) are performed in MACs after 5 days of differentiation. (**E**) Effects of TET2, TDG and AID downregulation on 5mC and 5hmC in OC differentiated during 20 days. Percentage of 5mC and 5hmC are evaluated in ANXA2, TM4SF19 and ADAM12 following siRNA downregulation of TET2 (upper rows), TDG (third row) and AID (lower row). (**F**) Analyses of gene expression of *ANXA2*, *TM4SF9* and *ADAM12* by RT-qPCR following siRNA downregulation of TET2 (upper row), TDG (middle row) and AID (lower row). Relative mRNA is normalized against *RPL38*.

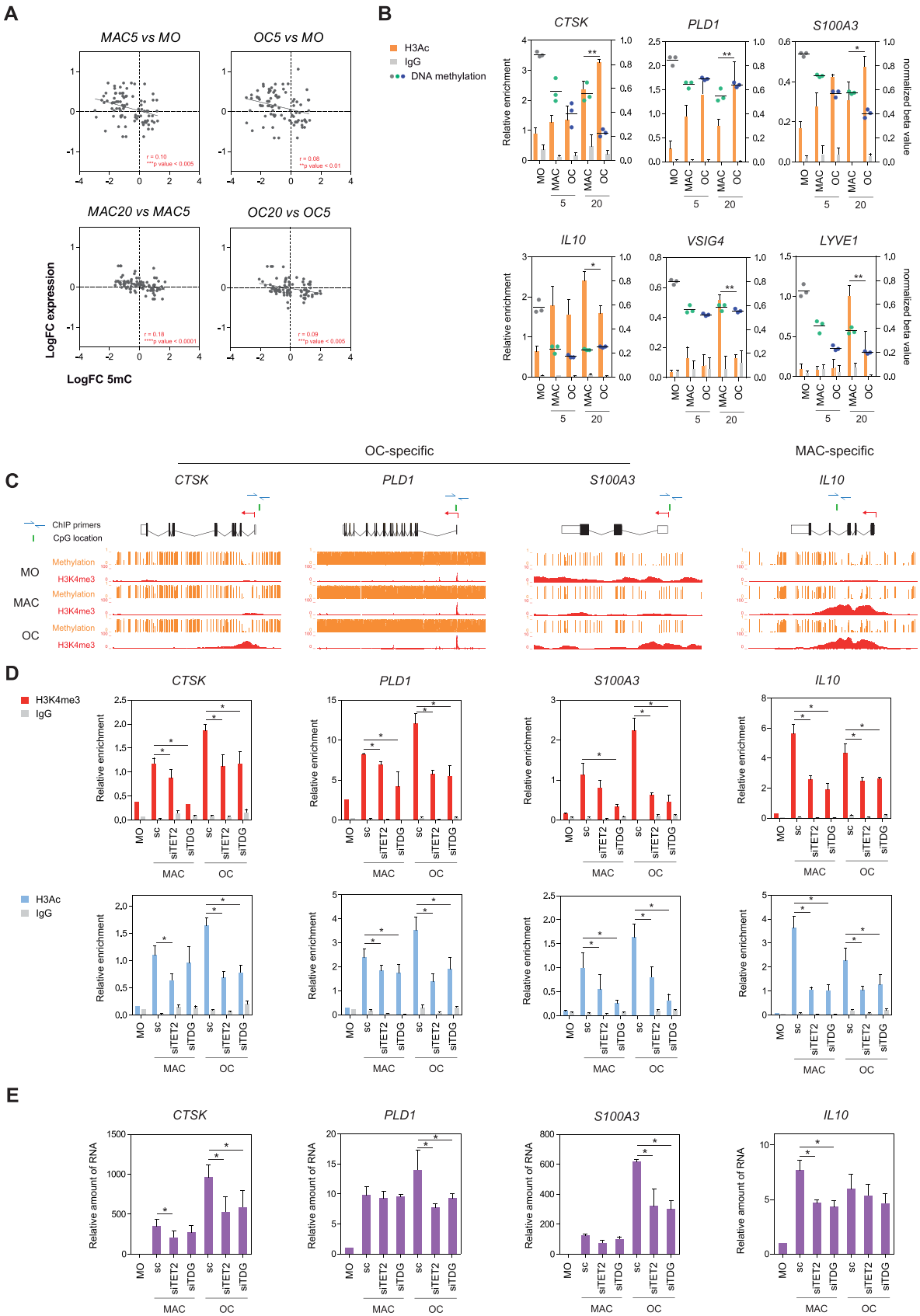

Figure 5. Relationship between TET2 and TDG participation and activating histone marks in MAC and OC differentiation. (**A**) Scatter plots depicting the correlations of 5mC and gene expression for the comparisons of MAC and OC versus MOs at 5 and 20 days of differentiation. Solid lines indicate

solely to M-CSF. Despite the absence of 5mC and 5hmC differences between MACs and OCs, our data supports the essential role of TET2 and TDG in the acquisition of expression changes that will lead to the generation of the differentiated phenotypes. Data by Michael Rehli and colleagues (27) previously proved the essential role of TET2 in demethylation processes from human monocytes. In this study, we show how TDG and AID are also determinant for the acquisition of key expression changes to yield the final phenotype. The participation of AID in active DNA demethylation has been controversial in the past few years (44,45), and it has been reported to involve the deamination of 5mC and 5hmC. In this respect, our data suggest a participation of AID in this process, although the detailed participation and gene specificity require further analysis.

Given that MACs and OCs display around 16.4% of differences in their expression profiles, this therefore suggests that alternative mechanisms, other than DNA methylation, are involved in their establishment. In our study, we prove that histone modifications are associated with the existence of differential expression of genes becoming demethylated. It is interesting to highlight that many of these genes that are differentially expressed between MACs and OCs undergo demethylation at a similar extent. In our study, we prove that demethylation of these genes leads to a competent state that is then sensitive to further epigenetic mechanisms in MACs and OCs, such as histone modifications. Additional mechanisms, like microRNA-mediated control may also play a part in differential gene expression. In fact, we have recently shown that NF-κB, downstream of RANKL, mediates the control of several microRNAs essential for OC and MAC differentiation (47). Our results provide evidence of the participation of active DNA demethylation machinery, focusing on TET2 and TDG, in determining changes not only in DNA methylation, but also in the recruitment of differential histone-modifying enzymes during MAC or OC differentiation. Previous studies have shown that TET proteins can interact indirectly with histone modifying complex SET1/COMPASS by promoting the OGT-mediated GlcNAcylation of the subunit HCF1 of the complex, favouring binding of SETD1A methyltransferase to chromatin and modulating H3K4me3 and subsequent transcriptional activation (24). We here prove that SETD1A binding to genes that demethylated and specifically expressed in OCs depend on TET2.

Other studies have shown that TDG interacts with activating histone modifiers such as MLL or CBP/p300 to maintain active H3K4me2-enriched chromatin states during cell differentiation, and preventing the gain of repressive H3K27 and H3K9 trimethylation and subsequent transcriptional silencing (26,48). Also, in OC differentiation, it has been reported that RANKL stimulates the recruitment of chromatin modifiers such as EZH2 or Jmjd3 to mediate H3K27 methylation changes in OC-specific genes (49,50). The selective TET2- and TDG-mediated recruitment of histone-modifying enzymes to target particular genomic regions suggests a specific mechanism that will need further investigation. Of note, RANKL-mediated regulation in modulating histone modifications relies not only on promoting genes that are more actively transcribed, but also on preventing activating histone marks to those genes that are upregulated in MAC differentiation such as *IL10*.

Furthermore, our results support the role of 5hmC as a stable epigenetic mark. This has been previously reported using stable isotope labeling of cytosine derivatives in the DNA of mammalian cells and ultrasensitive tandem liquid-chromatography mass spectrometry (16). However, our analysis represents the first report of the dynamics of these changes in immune cell differentiation. A significant proportion of the genes displaying high levels of 5hmC in MOs, which are rapidly lost during MAC and OC differentiation, encode for factors necessary for MOs. In addition, genes that undergo permanent gains of 5hmC during MAC and OC differentiation encode for key factors for both MACs and OCs. In this context, hydroxymethylation changes appear to account for core functions of MOs and these differentiated cells. Gain or loss of 5hmC could play a regulatory function through specific recruitment of 5hmC-binding proteins or 5hmC readers recently identified (19) that may promote transcription and chromatin accessibility.

Our findings shed light on the multiple roles of TET2 and TDG in determining the acquisition of the final phenotype on myeloid cells. We have demonstrated a direct role in the activation of genes that are commonly upregulated in two terminal differentiation processes. In addition, we prove that a common TET2- and TDG-mediated demethylation step is required to allow the participation of subsequent differential epigenetic mechanisms that will determine the specific activation of MAC- and OC-specific genes. In these divergent processes, the active DNA demethylation machinery can direct RANKL-dependent histone modification, affecting specific cell type-specific gene transcription and contributing to the final phenotype.

ACCESSION NUMBERS

Methylation array and expression array data for this publication have been deposited in the NCBI Gene Expression

←

the tendency and r and p values are annotated. (**B**) ChIP assays showing the levels of histone H3Ac in selected genes that display differential levels of expression between MACs and OCs and undergo DNA demethylation in MACs or OCs. IgG (grey bar) was used as a negative control. Data is shown as relative enrichment of the bound fraction with respect to the input DNA. Data is represented as mean values of four independent experiments ± SEM. Statistically significant tests are represented as $*P<0.05$ and $**P<0.01$. Corresponding 5mC DNA methylation is depicted as a dotted graph and data were obtained as described in Figure 2. (**C**) Examples showing methylation and H3K4me3 binding pattern (ChIPseq data from BluePrint) at the region neighbouring selected hypomethylated CpGs. The CpG displaying differential methylation (Illumina probe) between MO and MAC/OC is marked with a green bar. (**D**) Quantitative ChIP assays showing the effects of TET2- and TDG-silencing on H3K4me3 and H3Ac enrichment to hypomethylated genes in MACs and OCs. (**E**) Effects of TET2 and TDG downregulation on expression of H3Ac and H3K4me3-enriched regions that become demethylated and reached higher expression in OC (*CTSK*, *PLD1*, *S100A3*) or MAC (*IL10*). Data in D and E represent mean values ± SEM with three biological triplicates and significant tests are represented as $*P < 0.05$.

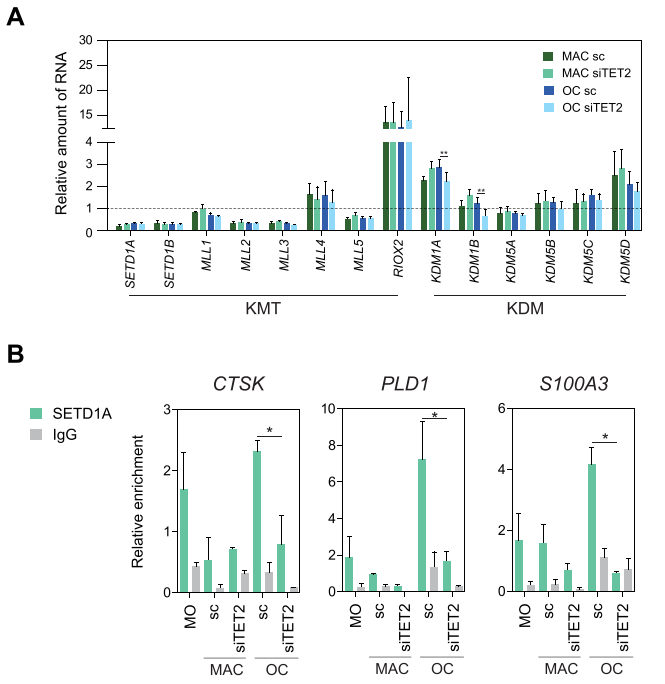

Figure 6. Effects of TET2 silencing on the expression and recruitment of H3K4 methyltransferases. (**A**) Gene expression analyses by qRT-PCR of several H3K4 methyltransferases (MLL1–5, SETD1A and SETD1B) and demethylases (KDM1A, KDM1B, KDM5A-D) following siRNA silencing of TET2 in MAC and OC at day 20 of differentiation. Gene expression was normalized against *RPL38* and a non-targeting siRNA was used as control. Expression of each gene was normalized against its expression in monocytes, indicated by the dotted line. (**B**) ChIP analyses of the recruitment of SETD1A to OC-specific genes, namely *CSTK*, *PLD1* and *S100A3*, in MAC and OC differentiated for 20 days upon TET2 silencing with siRNA. A non-targeting siRNA was used as a control and enrichment was compared to non-specific IgG binding. Experiments were performed as biological triplicates and significant tests are indicated as $*P < 0.05$ and $**P < 0.01$.

Omnibus and are accessible through GEO Series accession numbers GSE97497 and GSE97498.

SUPPLEMENTARY DATA

Supplementary Data are available at NAR Online.

FUNDING

Instituto de Salud Carlos III, an organisation of the Ministerio de Economía y Competitividad, and cofunding by FEDER funds/European Regional Development Fund (ERDF)—a way to build Europe [SAF2014-55942-R]; Multiple Myeloma Research Foundation (MMRF); Asociación Española Contra el Cáncer (AECC) (to A.G.G.). Funding for open access charge: Instituto de Salud Carlos III, an organisation of the Ministerio de Economía y Competitividad, and cofunding by FEDER funds/European Regional Development Fund (ERDF)—a way to build Europe [SAF2014-55942-R].
Conflict of interest statement. None declared.

REFERENCES

1. Tefferi,A., Lim,K.H., Abdel-Wahab,O., Lasho,T.L., Patel,J., Patnaik,M.M., Hanson,C.A., Pardanani,A., Gilliland,D.G. and Levine,R.L. (2009) Detection of mutant TET2 in myeloid malignancies other than myeloproliferative neoplasms: CMML, MDS, MDS/MPN and AML. *Leukemia*, **23**, 1343–1345.
2. Delhommeau,F., Dupont,S., Della Valle,V., James,C., Trannoy,S., Massé,A., Kosmider,O., Le Couedic,J.P., Robert,F., Alberdi,A. *et al.* (2009) Mutation in TET2 in myeloid cancers. *N. Engl. J. Med.*, **360**, 2289–2301.
3. Ley,T.J., Ding,L., Walter,M.J., McLellan,M.D., Lamprecht,T., Larson,D.E., Kandoth,C., Payton,J.E., Baty,J., Welch,J. *et al.* (2010) DNMT3A mutations in acute myeloid leukemia. *N. Engl. J. Med.*, **363**, 2424–2433.
4. Jones,P.A. (2012) Functions of DNA methylation: islands, start sites, gene bodies and beyond. *Nat. Rev. Genet.*, **13**, 484–492.
5. Shen,L., Wu,H., Diep,D., Yamaguchi,S., D'Alessio,A.C., Fung,H.L., Zhang,K. and Zhang,Y. (2013) Genome-wide analysis reveals TET- and TDG-dependent 5-methylcytosine oxidation dynamics. *Cell*, **153**, 692–706.
6. Bhutani,N., Brady,J.J., Damian,M., Sacco,A., Corbel,S.Y. and Blau,H.M. (2010) Reprogramming towards pluripotency requires AID-dependent DNA demethylation. *Nature*, **463**, 1042–1047.
7. Dominguez,P.M., Teater,M., Chambwe,N., Kormaksson,M., Redmond,D., Ishii,J., Vuong,B., Chaudhuri,J., Melnick,A. and Vasanthakumar,A. (2015) DNA methylation dynamics of germinal center B cells are mediated by AID. *Cell Rep.*, **12**, 2086–2098.
8. Guo,J.U., Su,Y., Zhong,C., Ming,G.L. and Song,H. (2011) Hydroxylation of 5-methylcytosine by TET1 promotes active DNA demethylation in the adult brain. *Cell*, **145**, 423–434.
9. Hashimoto,H., Zhang,X. and Cheng,X. (2012) Excision of thymine and 5-hydroxymethyluracil by the MBD4 DNA glycosylase domain: structural basis and implications for active DNA demethylation. *Nucleic Acids Res.*, **40**, 8276–8284.
10. Schomacher,L, Han,D, Musheev,M.U., Arab,K., Kienhöfer,S., von Seggern,A. and Niehrs,C. (2016) Neil DNA glycosylases promote substrate turnover by Tdg during DNA demethylation. *Nat. Struct. Mol. Biol.*, **23**, 116–124.
11. Hendrich,B. and Bird,A. (1998) Identification and characterization of a family of mammalian methyl-CpG binding proteins. *Mol. Cell. Biol.*, **18**, 6538–6547.
12. Prokhortchouk,A., Hendrich,B., Jørgensen,H., Ruzov,A., Wilm,M., Georgiev,G., Bird,A. and Prokhortchouk,E. (2001). The p120 catenin partner Kaiso is a DNA methylation-dependent transcriptional repressor. *Genes Dev.*, **15**, 1613–1618.
13. Jones,P.L., Veenstra,G.J., Wade,P.A., Vermaak,D., Kass,S.U., Landsberger,N., Strouboulis,J. and Wolffe,A.P. (1998) Methylated DNA and MeCP2 recruit histone deacetylase to repress transcription. *Nat Genet.*, **19**, 187–191.
14. Wade,P.A., Gegonne,A., Jones,P.L., Ballestar,E., Aubry,F. and Wolffe,A.P. (1999) Mi-2 complex couples DNA methylation to chromatin remodelling and histone deacetylation. *Nat. Genet.*, **23**, 62–66.
15. Wagner,M, Steinbacher,J, Kraus,TF, Michalakis,S, Hackner,B, Pfaffeneder,T, Perera,A., Müller,M., Giese,A., Kretzschmar,H.A. *et al.* (2015) Age-dependent levels of 5-methyl-, 5-hydroxymethyl-, and 5-formylcytosine in human and mouse brain tissues. *Angew. Chem. Int. Ed. Engl.*, **54**, 12511–11254.
16. Bachman,M., Uribe-Lewis,S., Yang,X., Williams,M., Murrell,A. and Balasubramanian,S. (2014) 5-Hydroxymethylcytosine is a predominantly stable DNA modification. *Nat. Chem.*, **6**, 1049–1055.
17. Valinluck,V., Tsai,H.H., Rogstad,D.K., Burdzy,A., Bird,A. and Sowers,L.C. (2004) Oxidative damage to methyl-CpG sequences inhibits the binding of the methyl-CpG binding domain (MBD) of methyl-CpG binding protein 2 (MeCP2). *Nucleic Acids Res.*, **32**, 4100–4108.
18. Sayeed,S.K., Zhao,J., Sathyanarayana,B.K., Golla,J.P. and Vinson,C. (2015) C/EBPβ (CEBPB) protein binding to the C/EBP|CRE DNA 8-mer TTGC|GTCA is inhibited by 5hmC and enhanced by 5mC, 5fC, and 5caC in the CG dinucleotide. *Biochim. Biophys. Acta*, **1849**, 583–589.
19. Spruijt,C.G., Gnerlich,F., Smits,A.H., Pfaffeneder,T., Jansen,P.W., Bauer,C., Münzel,M., Wagner,M., Müller,M., Khan,F. *et al.* (2013)

Dynamic readers for 5-(hydroxy)methylcytosine and its oxidized derivatives. *Cell*, **152**, 1146–1159.
20. Bachman,M., Uribe-Lewis,S., Yang,X., Burgess,H.E., Iurlaro,M., Reik,W., Murrell,A. and Balasubramanian,S. (2015) 5-Formylcytosine can be a stable DNA modification in mammals. *Nat. Chem. Biol.*, **11**, 555–557.
21. Iurlaro,M., Ficz,G., Oxley,D., Raiber,E.A., Bachman,M., Booth,M.J., Andrews,S., Balasubramanian,S. and Reik,W. (2013) A screen for hydroxymethylcytosine and formylcytosine binding proteins suggests functions in transcription and chromatin regulation. *Genome Biol.*, **14**, R119.
22. Iurlaro,M., McInroy,G.R., Burgess,H.E., Dean,W., Raiber,E.A., Bachman,M., Beraldi,D., Balasubramanian,S. and Reik,W. (2016) In vivo genome-wide profiling reveals a tissue-specific role for 5-formylcytosine. *Genome Biol.*, **17**, 141.
23. Klug,M., Heinz,S., Gebhard,C., Schwarzfischer,L., Krause,S.W., Andreesen,R. and Rehli,M. (2010) Active DNA demethylation in human postmitotic cells correlates with activating histone modifications, but not transcription levels. *Genome Biol.*, **11**, R63.
24. Deplus,R., Delatte,B., Schwinn,M.K., Defrance,M., Méndez,J., Murphy,N., Dawson,M.A., Volkmar,M., Putmans,P., Calonne,E. *et al.* (2013) TET2 and TET3 regulate GlcNAcylation and H3K4 methylation through OGT and SET1/COMPASS. *EMBO J.*, **32**, 645–655.
25. Wu,H., D'Alessio,A.C., Ito,S., Xia,K., Wang,Z., Cui,K., Zhao,K., Sun,Y.E. and Zhang,Y. (2011) Dual functions of Tet1 in transcriptional regulation in mouse embryonic stem cells. *Nature*, **473**, 389–393.
26. Cortázar,D., Kunz,C., Selfridge,J., Lettieri,T., Saito,Y., MacDougall,E., Wirz,A., Schuermann,D., Jacobs,A.L., Siegrist,F. *et al.* (2011) Embryonic lethal phenotype reveals a function of TDG in maintaining epigenetic stability. *Nature*, **470**, 419–423.
27. Klug,M., Schmidhofer,S., Gebhard,C., Andreesen,R. and Rehli,M. (2013) 5-Hydroxymethylcytosine is an essential intermediate of active DNA demethylation processes in primary human monocytes. *Genome Biol.*, **14**, R46.
28. Vento-Tormo,R., Company,C., Rodríguez-Ubreva,J., de la Rica,L., Urquiza,J.M., Javierre,B.M., Sabarinathan,R., Luque,A., Esteller,M., Aran,J.M. *et al.* (2016) IL-4 orchestrates STAT6-mediated DNA demethylation leading to dendritic cell differentiation. *Genome Biol.*, **17**, 4.
29. de la Rica,L, Rodríguez-Ubreva,J., García,M., Islam,A.B., Urquiza,J.M., Hernando,H., Christensen,J., Helin,K., Gómez-Vaquero,C. and Ballestar,E. (2013) PU.1 target genes undergo Tet2-coupled demethylation and DNMT3b-mediated methylation in monocyte-to-osteoclast differentiation. *Genome Biol.*, **14**, R99.
30. Booth,M.J., Ost,T.W., Beraldi,D., Bell,N.M., Branco,M.R., Reik,W. and Balasubramanian,S. (2013) Oxidative bisulfite sequencing of 5-methylcytosine and 5-hydroxymethylcytosine. *Nat. Protoc.*, **8**, 1841–1851.
31. Al-Shahrour,F., Díaz-Uriarte,R. and Dopazo,J. (2004) FatiGO: a web tool for finding significant associations of Gene Ontology terms with groups of genes. *Bioinformatics*, **20**, 578–580.
32. Kondo,Y., Yasui,K., Yashiro,M., Tsuge,M., Kotani,N. and Morishima,T. (2009) Multi-nucleated giant cell formation from human cord blood monocytes in vitro, in comparison with adult peripheral blood monocytes. *Clin. Exp. Immunol.* **158**, 84–90.
33. Kittan,N.A., Allen,R.M., Dhaliwal,A., Cavassani,K.A., Schaller,M., Gallagher,K.A., Carson,W.F., Mukherjee,S., Grembecka,J., Cierpicki,T. *et al.* (2013) Cytokine induced phenotypic and epigenetic signatures are key to establishing specific macrophage phenotypes. *PLoS One*, **8**, e78045.
34. Zhao,B. and Ivashkiv,L.B. (2011) Negative regulation of osteoclastogenesis and bone resorption by cytokines and transcriptional repressors. *Arthritis Res. Ther.*, **13**, 234.
35. Søndergaard,J.N., Poghosyan,S., Hontelez,S., Louche,P., Looman,M.W., Ansems,M. and Adema,G.J. (2015) DC-SCRIPT regulates IL-10 production in human dendritic cells by modulating NF-κBp65 activation. *J. Immunol.*, **195**, 1498–1505.
36. Kühnemuth,B., Mühlberg,L., Schipper,M., Griesmann,H., Neesse,A., Milosevic,N., Wissniowski,T., Buchholz,M., Gress,T.M. and Michl,P. (2015) CUX1 modulates polarization of tumor-associated macrophages by antagonizing NF-κB signaling. *Oncogene*, **34**, 177–187.
37. Cai,J, Li,R, Xu,X, Zhang,L, Wu,S, Yang,T, Fang,L., Wu,J., Zhu,X., Li,M. *et al.* (2015) URGCP promotes non-small cell lung cancer invasiveness by activating the NF-κB-MMP-9 pathway. *Oncotarget*, **6**, 36489–36504.
38. Booth,M.J., Branco,M.R., Ficz,G., Oxley,D., Krueger,F., Reik,W. and Balasubramanian,S. (2012) Quantitative sequencing of 5-methylcytosine and 5-hydroxymethylcytosine at single-base resolution. *Science*, **336**, 934–937.
39. Yu,M., Hon,G.C., Szulwach,K.E., Song,C.X., Zhang,L., Kim,A., Li,X., Dai,Q., Shen,Y., Park,B. *et al.* (2012) Base-resolution analysis of 5-hydroxymethylcytosine in the mammalian genome. *Cell*, **149**, 1368–1380.
40. Lunnon,K., Hannon,E., Smith,R.G., Dempster,E., Wong,C., Burrage,J., Troakes,C., Al-Sarraj,S., Kepa,A., Schalkwyk,L. *et al.* (2016) Variation in 5-hydroxymethylcytosine across human cortex and cerebellum. *Genome Biol.*, **17**, 27.
41. Jin,S.G., Wu,X., Li,A.X. and Pfeifer,G.P. (2011) Genomic mapping of 5-hydroxymethylcytosine in the human brain. *Nucleic Acids Res.*, **39**, 5015–5024.
42. Hahn,M.A., Qiu,R., Wu,X., Li,A.X., Zhang,H., Wang,J., Jui,J., Jin,S.G., Jiang,Y., Pfeifer,G.P. *et al.* (2013) Dynamics of 5-hydroxymethylcytosine and chromatin marks in Mammalian neurogenesis. *Cell Rep.*, **3**, 291–300.
43. Laurent,L., Wong,E., Li,G., Huynh,T., Tsirigos,A., Ong,C.T., Low,H.M., Kin Sung,K.W., Rigoutsos,I., Loring,J. *et al.* (2010) Dynamic changes in the human methylome during differentiation. *Genome Res.*, **20**, 320–331.
44. Cortellino,S., Xu,J., Sannai,M., Moore,R., Caretti,E., Cigliano,A., Le Coz,M., Devarajan,K., Wessels,A., Soprano,D.. *et al.* (2011) Thymine DNA glycosylase is essential for active DNA demethylation by linked deamination-base excision repair. *Cell*, **146**, 67–79.
45. Nabel,C.S., Jia,H., Ye,Y., Shen,L., Goldschmidt,H.L., Stivers,J.T., Zhang,Y. and Kohli,R.M. (2012) AID/APOBEC deaminases disfavor modified cytosines implicated in DNA demethylation. *Nat. Chem. Biol.*, **8**, 751–758.
46. Xue,J.H., Xu,G.F., Gu,T.P., Chen,G.D., Han,B.B., Xu,Z.M., Bjørås,M., Krokan,H.E., Xu,G.L. and Du,Y.R. (2016) Uracil-DNA glycosylase UNG promotes Tet-mediated DNA demethylation. *J. Biol. Chem.*, **291**, 731–738.
47. de la Rica,L., García-Gómez,A., Comet,N.R., Rodríguez-Ubreva,J., Ciudad,L., Vento-Tormo,R., Company,C., Álvarez-Errico,D., García,M., Gómez-Vaquero,C. *et al.* (2015) NF-κB-direct activation of microRNAs with repressive effects on monocyte-specific genes is critical for osteoclast differentiation. *Genome Biol.*, **16**, 2.
48. Tini,M., Benecke,A., Um,S.J., Torchia,J., Evans,R.M. and Chambon,P. (2002) Association of CBP/p300 acetylase and thymine DNA glycosylase links DNA repair and transcription. *Mol. Cell*, **9**, 265–277.
49. Fang,C., Qiao,Y., Mun,S.H., Lee,M.J., Murata,K., Bae,S., Zhao,B., Park-Min,K.H. and Ivashkiv,L.B. (2016) Cutting edge: EZH2 promotes osteoclastogenesis by epigenetic silencing of the negative regulator IRF8. *J. Immunol.*, **196**, 4452–4456.
50. Yasui,T., Hirose,J., Tsutsumi,S., Nakamura,K., Aburatani,H. and Tanaka,S. (2011) Epigenetic regulation of osteoclast differentiation: possible involvement of Jmjd3 in the histone demethylation of Nfatc1. *J. Bone Miner. Res.*, **26**, 2665–2671.